Characteristics of Two-Dimensional Quantum Turbulence in a Compressible Superfluid

T. W. Neely,[1,*] A. S. Bradley,[2,†] E. C. Samson,[1] S. J. Rooney,[2] E. M. Wright,[1] K. J. H. Law,[3] R. Carretero-González,[4] P. G. Kevrekidis,[5] M. J. Davis,[6] and B. P. Anderson[1,‡]

[1]*College of Optical Sciences, University of Arizona, Tucson, Arizona 85721, USA*
[2]*Jack Dodd Centre for Quantum Technology, Department of Physics, University of Otago, Dunedin 9016, New Zealand*
[3]*Mathematics Institute, University of Warwick, Coventry CV4 7AL, United Kingdom*
[4]*Department of Mathematics and Statistics, San Diego State University, San Diego, California 92182, USA*
[5]*Department of Mathematics and Statistics, University of Massachusetts, Amherst, Massachusetts 01003, USA*
[6]*School of Mathematics and Physics, University of Queensland, Brisbane, Queensland 4072, Australia*

(Received 14 August 2013; published 2 December 2013)

Fluids subjected to suitable forcing will exhibit turbulence, with characteristics strongly affected by the fluid's physical properties and dimensionality. In this work, we explore two-dimensional (2D) quantum turbulence in an oblate Bose-Einstein condensate confined to an annular trapping potential. Experimentally, we find conditions for which small-scale stirring of the condensate generates disordered 2D vortex distributions that dissipatively evolve toward persistent currents, indicating energy transport from small to large length scales. Simulations of the experiment reveal spontaneous clustering of same-circulation vortices and an incompressible energy spectrum with $k^{-5/3}$ dependence for low wave numbers k. This work links experimentally observed vortex dynamics with signatures of 2D turbulence in a compressible superfluid.

DOI: 10.1103/PhysRevLett.111.235301 PACS numbers: 67.85.De, 03.75.Lm, 67.25.dk

A distinction between hydrodynamic turbulence [1] in a bulk fluid and in one whose flows are restricted to two dimensions is that energy dissipation at small length scales is inhibited in the latter. In two-dimensional (2D) flows subject to small-scale forcing, energy flux toward shorter scales is suppressed and, instead, kinetic energy is transported toward larger scales. These dynamics lead to the well-known inverse energy cascade [2,3]. Small-scale forcing may thus generate large-scale flows in effectively 2D fluids, as seen, for instance, in atmospheric strata [4], electrolyte solutions and toroidal plasmas [5], and Jupiter's Great Red Spot [6,7]. However, analogous characteristics involving vortex distributions [8] and energy spectra of 2D turbulence in *quantum* fluids are less clear: 2D quantum turbulence (2DQT) has only recently been addressed theoretically [9–17], while an experimental demonstration of 2DQT has remained elusive.

Here, we study an atomic Bose-Einstein condensate (BEC), a compressible superfluid, in a joint experimental and numerical investigation of forced and decaying 2DQT. We demonstrate that 2DQT is readily generated in BECs and that the disordered vortex distributions of 2DQT can be robust against immediate vortex-antivortex annihilation. Our primary result is evidence that quantum-fluid analogs of three key characteristics of classical 2D turbulence can simultaneously appear in 2DQT: (i) emergence of disordered vortex distributions following small-scale forcing, decaying into large-scale flow as manifested by a persistent current, seen experimentally and numerically; (ii) formation of coherent vortex structures, observed numerically; and (iii) an incompressible kinetic energy spectrum with $k^{-5/3}$ dependence for wave numbers k lower than that of the forcing, observed numerically.

To experimentally generate 2DQT, we utilize optical and magnetic confinement to create highly oblate BECs [18]. A harmonic potential with radial (r) and axial (z) trapping frequencies $(\omega_r/2\pi, \omega_z/2\pi) = (8, 90)$ Hz confines BECs of up to $\sim 2 \times 10^6$ ^{87}Rb atoms, with radial and axial Thomas-Fermi radii $(R_r, R_z) = (52, 5)$ μm and chemical potentials $\mu_0 \sim 8\hbar\omega_z$. For these conditions, vortex bending and tilting are suppressed [19], enabling 2D vortex dynamics [20]. Additionally, a 23-μm, $1/e^2$-radius, blue-detuned Gaussian laser beam is directed axially through the trap, creating an annular trap with a central barrier of height $\sim 1.5\mu_0$. At time $t = 0$, a magnetic bias field moves the harmonic trap center, but not the barrier, in a 5.7-μm-diameter circle over 333 ms. This motion induces nucleation of numerous vortices in a highly disordered distribution, identified with 2DQT much as the notion of a "vortex tangle" is identified with 3D quantum turbulence [21–24]. The BEC then remains in the annular trap for a variable hold time $t_h \leq 50$ s while the 2DQT decays. The barrier is then ramped off over 250 ms, and the BEC is released from the trap to ballistically expand, enabling the absorption imaging of vortices. Figure 1 illustrates this sequence.

Two experimental sequences of poststir dynamics are shown in Figs. 2(a) and 2(b), revealing the microscopic variability of vortex distributions. From the data, we discover the following new regimes of vortex dynamics. First, small-scale stirring generates numerous (> 20) vortices, which are then rapidly distributed, creating a disordered

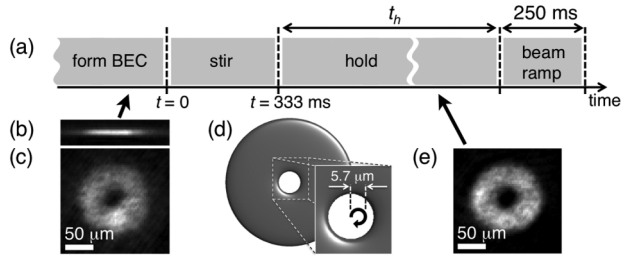

FIG. 1. (a) Timing sequence. (b,c) *In situ* BEC column-density images prior to the stir, shown (b) in the plane of 2D trapping and (c) along the z axis. Lighter shades indicate larger column densities, as in subsequent data. (d) Stirring illustration. The black arrow shows the trap center trajectory relative to the larger fluid-free region created by the laser barrier. (e) *In situ* BEC image 10 s after stirring.

distribution associated with 2DQT by the end of the stir ($t_h = 0$ ms). Second, vortex decay rates via annihilation and damping are slow compared with stirring times. Third, the vortex cores maintain high visibility, indicating that vortices remain aligned along the trap's axial direction and that the BEC's velocity field and vortex dynamics are 2D despite the fluid's 3D nature, Kelvin wave dynamics being suppressed for our 2D forcing and trap anisotropy [19].

A fourth phenomenon is the stable pinning [25] of vortices at the central barrier accompanying the 2DQT decay, indicated by the large fluid-free hole in the expanded BEC's center for $t_h > 0.33$ s. By $t_h \sim 8.17$ s, after the 2DQT has decayed, we observe that a persistent current has formed, visible for up to $t_h = 50$ s. By ramping off the central barrier prior to BEC expansion, pinned

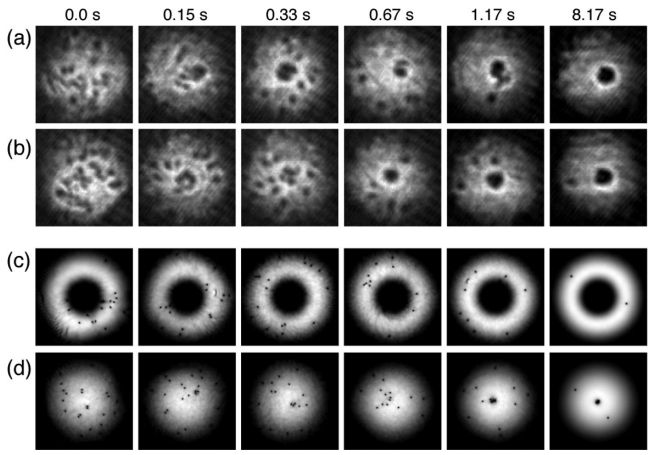

FIG. 2. (a,b) 200-μm-square experimental column-density images acquired at the hold times t_h indicated. BECs undergo ~50-ms ballistic expansion immediately after barrier removal. Each image is acquired from a separate experimental run. (c) *In situ* numerical data (96-μm-square images) for the hold times indicated. See also Movie S1 in the Supplemental Material [28]. For each state represented in (c), ramping off the laser barrier in 250 ms gives the data shown in (d).

vortices are released into the BEC [26,27], permitting their imaging. An optional 3-s hold before expansion gives the vortices time to separate, allowing determination of the persistent current winding number [26] (see the Supplemental Material [28]). Our data show that the persistent current forms during the dissipative vortex dynamics, rather than being directly created by the stirring process. In interpreting this phenomenon, we note the following. First, prior to stirring, the system is stationary; thus, the rotating trap mode that corresponds to the eventual annular superflow is initially unpopulated. Second, stirring injects kinetic energy at small scales (discussed below) but does not inject energy directly into the large-scale rotating trap mode that corresponds to the persistent current. Although stirring *is* responsible for the injection of angular momentum, which is initially embedded in the vortex distribution, the macroscopic rotation emerges from the subsequent vortex dynamics. We interpret the emergence of annular superflow as an experimental signature of energy transport from small to large length scales during 2DQT forcing and decay.

The decay of 2DQT is not necessary to create annular superflow, as methods for direct BEC persistent current creation have been demonstrated elsewhere [26,29,30]. The decay of 2DQT in an annular trap is also not sufficient to guarantee the formation of a persistent current, and an important parameter of our experiment is the BEC temperature, on which the superfluid dynamics strongly depend. Prior to forcing, the initial temperature is $T \sim 0.9T_c$, where $T_c \sim 116$ nK is the BEC phase-transition temperature. We choose this relatively high temperature so that the acoustic energy generated by the forcing undergoes efficient thermal damping. We find that for temperatures much above this value, most vortices quickly decay, while much lower temperatures inhibit the establishment of a persistent current. By $t_h = 1.17$ s, most of the vortices have become pinned to the central barrier or have left the system by annihilation and damping. At this time, we reduce the temperature to $\sim 0.6T_c$ by additional evaporative cooling in order to decrease rates of further thermal damping. The temperatures used during the forcing and decay stages were experimentally chosen to optimize persistent current formation from 2DQT decay. The role of dissipation has elsewhere been shown to be important in the development of a turbulent energy spectrum [16,31], and we return to this topic and aspects of system dimensionality near the end of this Letter. Our experiment thus demonstrates that under suitable conditions of system geometry, forcing, and dissipation, a disordered 2D vortex distribution can form and dissipatively evolve into a large-scale flow. These experimental results establish atomic BECs as a promising platform for further studies of 2DQT. Nevertheless, measuring energy spectra and vortex dynamics remain forefront experimental challenges, motivating us to utilize numerical modeling and analysis to

investigate these characteristics of 2DQT in a stirred and trapped BEC.

Weakly interacting BECs admit a numerically tractable first-principles theoretical approach, across a broad range of temperatures, that has compared favorably and quantitatively with experiments [32]. The physical system consists of a large noncondensate component close to thermal equilibrium and a BEC responding to both external forcing and damping by the noncondensate component. Numerically, we focus on the BEC dynamics, simulating the experimental procedure using damped Gross-Pitaevskii theory [28,33].

Figure 2(c) and Movie S1 in the Supplemental Material [28] show results from simulations that correspond to experimental conditions. We see that vortices are rapidly generated near the inner BEC boundary and subsequently dispersed, with some becoming pinned to the central barrier. At $t_h = 8.17$ s, three vortices are pinned. Consistent with experimental observations, we find that over the first few seconds of evolution after the stir ends, large-scale azimuthal flow and hence a persistent current steadily build due to the redistribution of vortices rather than being directly imprinted by the stir; see Fig. S1 [28]. Ramping off the barrier in the simulation over 250 ms gives the column densities shown in Fig. 2(d), with disordered vortex distributions qualitatively similar to Figs. 2(a) and 2(b). The development of superflow by $t_h = 8.17$ s in Fig. 2(c) leads to a large region of low density in the trap center after barrier ramp-down, as seen in Figs. 2(a), 2(b), and 2(d). The mean number of vortices (pinned and free) for $t_h = 23$ s is 3.5 in the experiment and 5 in the simulation. For $t_h = 43$ s, these values decline to 2.5 and 3, respectively.

Energy spectra and vortex distribution [8] analyses further characterize 2DQT. To examine the dependence of the kinetic energy on k at any time, we use techniques of previous studies [10–13,34] for extracting $E^i(k)$, the portion of a BEC's kinetic energy spectrum corresponding to an incompressible superfluid component, derived by extracting the divergence-free density-weighted velocity field that embeds vorticity [35]. The curl-free part of this field embeds acoustic energy, which reaches a maximum value equivalent to 40% of the total incompressible energy halfway through the stir, dropping to less than 20% by the end of the stir and for subsequent times.

The spectra of Fig. 3 are obtained from various times of the simulation and calculated using spatial grids of 1811^2 points separated by $\xi/4 = 0.1$ μm, where $\xi = 0.42$ μm is the healing length at peak density. Each curve shows the spectrum of a 2D slice through $z = 0$, although the spectra are only negligibly changed by averaging over slices. As stirring injects kinetic energy into the system, a $k^{-5/3}$ power-law spectrum develops in the $k < k_s \equiv \xi^{-1}$ region. Remarkably, this power law is consistent with Kolmogorov's analysis of turbulence spectra [36] in spite of the fact that the ideal conditions of isotropic and

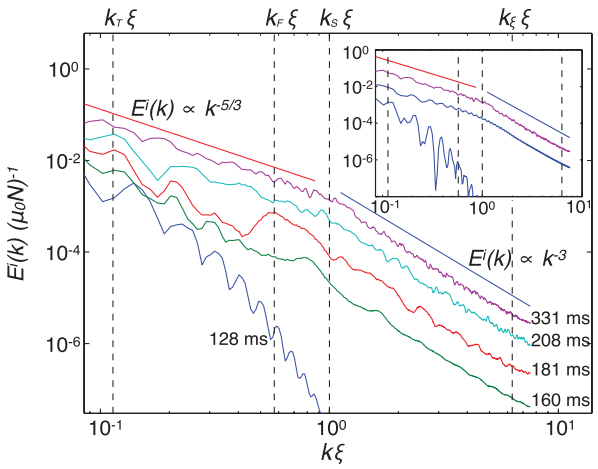

FIG. 3 (color). Log-log plots of $E^i(k)$ (per atom) vs $k\xi$ during forcing, for the times indicated. Vertical dashed lines indicate k_T, k_F, k_s, and k_ξ, defined in the text. The straight red and blue lines indicate $E^i(k) \propto k^{-5/3}$ and k^{-3}, respectively. Inset: Log-log plot of $E^i(k)$ vs $k\xi$ (labels omitted) for decaying 2DQT. Straight lines show $E^i(k) \propto k^{-5/3}$ and k^{-3}. From top to bottom, the remaining three curves show $E^i(k)$ at 331 ms, after 14 s of free decay, and for a charge-three persistent current.

homogeneous turbulence are not satisfied in the present case. For 2DQT, this spectrum is determined by the vortex configuration [14]. This spectrum spans a decade in k space and is established by the end of the stir, which is also when total incompressible kinetic energy is maximal. Poststir, Fig. 3 (inset) indicates a slow loss of energy with approximate preservation of the $k^{-5/3}$ power law. Eventually, the system populates the mode associated with a persistent current with three units of circulation.

The logarithmically bilinear spectrum is a robust dynamical feature, with the ultraviolet (large k) $E^i(k) \propto k^{-3}$ dependence emerging once vortices are present. Because the fluid's compressibility determines the vortex core structure, this portion of the spectrum is a universal property of isolated quantized vortices in a compressible 2D quantum fluid, occurring for $k > k_s$ [14]. This ultraviolet power law only plays a role in the energy spectrum through its amplitude, which is proportional to the total vortex number. For $k \sim k_s$, fluid compressibility provides a mechanism for the conversion of vortices into sound [14] (see the Supplemental Material [28]). Conservation of enstrophy (mean-squared vorticity) is therefore complicated by vortex-antivortex annihilation, since in 2DQT, enstrophy corresponds to vortex number [11,14]. The flux of kinetic energy from large to small k that would lead to the development of a $k^{-5/3}$ power law in this system is thus not *a priori* expected. Logarithmically bilinear spectra are also obtained after ramping off the central barrier, indicating that these spectra are robust and that an annular geometry is not a necessary element of $k^{-5/3}$ spectra in 2DQT.

Three additional wave numbers are indicated in Fig. 3. The cross-sectional radial thickness of the toroidal BEC approximately corresponds to the length scale 25 μm $= 2\pi/k_T$. At high wave numbers, $k_\xi = 2\pi/\xi$ corresponds to the approximate size of the smallest features supported by a BEC. In an isotropic BEC, ξ is roughly the distance from the vortex core center to a location at which the density is approximately half its bulk value. Finally, a wave number k_F is associated with a forcing scale. In the classical theory of 2D turbulence [3], spectrally localized forcing is related to the injection rates of enstrophy (η) and energy (ϵ) density via $k_F = \sqrt{\eta/\epsilon}$ [1]. We estimate k_F from the computed changes in total incompressible kinetic energy $\Delta E^i \approx 2.9 \times 10^{-3}\mu_0 N$ and enstrophy $\Delta\Omega \approx 0.963 \times 10^{-3}\mu_0 N/\xi^2$ occurring between 181 and 208 ms (see the Supplemental Material [28]). We find $k_F \equiv \sqrt{\Delta\Omega/\Delta E^i} = 0.57\xi^{-1} \simeq 2\pi/(11\xi)$, shown in Fig. 3, and see that this scale coincides with a spectral peak that appears near $k\xi \sim 2\pi/11$ at 181 ms. The peak disperses by 208 ms when the spectrum is already approximately logarithmically bilinear. We therefore interpret k_F as an approximate forcing-scale wave number.

The physical mechanism for the injection of energy and vorticity into our BECs involves coupling between pairs of opposite-circulation vortices and acoustic energy. Empirically, we find that the length scale $\sim 2\pi/k_F$ coincides with the separation of phase singularities created from the decay of localized sound pulses into vortex dipoles, visible in Movie S1 [28]. We find analytic evidence (see the Supplemental Material [28]) for the efficient energy and enstrophy transfer from the compressible to the incompressible fluid components for wave numbers $k_F \lesssim k \lesssim k_s$, supporting the interpretation that forcing occurs near k_F.

The spatial clustering of same-circulation vortices is a key characteristic of 2DQT, first discussed by Onsager [8]. More recently, vortex clusters in 2DQT have been examined in order to better understand their contributions to kinetic energy spectra and as analogs of the coherent vortices of classical 2D turbulence [14]. Vortex clustering is amenable to quantitative analysis, as discussed in Refs. [14,16,37]. Although these measures apply to 2D vortex distributions in homogeneous superfluids, we apply the algorithm described in Ref. [16] to estimate the degree of vortex clustering in our results, noting that we must neglect corrections due to the system geometry and density inhomogeneities (see the Supplemental Material [28]). During the 300-ms period after the stir, we observe four tightly bound two-vortex clusters, visible in Movie S1 [28]. Applying the cluster algorithm of Ref. [16], some of these pairs appear as elements of larger clusters. Figure 4 shows the identified vortex dipoles and clusters for three times immediately before and after the stir ends. The two-vortex cluster indicated by the dashed red line in the rightmost plot exists for 630 ms. These vortices orbit each other 15 times, travel together halfway around the BEC, and eventually dissociate upon colliding with a vortex dipole; see Movie S1 [28]. At the end of the stir, the fraction of free vortices involved in clusters is $\sim$0.65, whereas this measure would be 0.5 for a completely uncorrelated vortex distribution and well below 0.5 for a system dominated by vortex dipoles [38]. We conclude that vortices are likely not randomly distributed and that vortex clustering dynamically occurs during forcing and is maintained even after forcing stops.

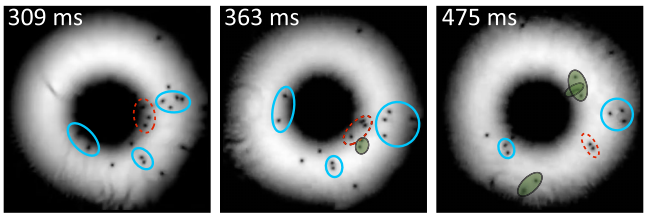

FIG. 4 (color online). Numerical 96-μm-square column-density plots shown for times after the start of the 333-ms stir. Solid blue (dashed red) ovals indicate clusters of same-sign vortices counterrotating (corotating) with the stir direction. Vortex dipoles are indicated by shaded green ovals. Unlabeled vortices are not identifiable as part of a dipole or cluster. See Fig. S4 in the Supplemental Material [28] for phase plots.

We have also performed experiments and simulations to further explore the roles of dissipation and dimensionality. Similar experiments in oblate traps with $\omega_z : \omega_r = 2:1$ showed substantially fewer vortices generated initially and a rapid decrease of vortex visibility likely due to vortex annihilation, damping, and bending. The trap oblateness and the stirring still retain aspects of 2D superfluid dynamics, and experimental parameters were found for which persistent currents were formed, suggesting that a wider range of conditions may be suitable for 2DQT studies. To probe the consequences of stirring in a spherically symmetric ($\omega_r = \omega_z$) trap, we performed simulations using stirring and dissipation parameters comparable to the highly oblate case. Here, however, we observed neither vortices nor a persistent current (see the Supplemental Material [28]), and instead the BEC rapidly returns to nonrotating equilibrium. Without dissipation, vortices are not nucleated, and the 3D BEC develops a transverse sloshing mode in response to the stir. We also simulated the stir sequence for the highly oblate system, but without dissipation. Vortex nucleation and short-time dynamics are qualitatively comparable to the dissipative calculation, with the notable difference that thermalization occurs in the nonlinear Gross-Pitaevskii equation evolution via coupling between vortices and the sound field, a consequence of compressibility. The time scale of persistent current formation is much longer than that of our dissipative simulations and experiments. We infer that 2D vortex dynamics and dissipation are both required for small-scale forcing to efficiently produce large-scale flow in the annular trap.

While previous numerical 2DQT studies have investigated energy spectra and vortex dynamics, relationships with classical 2D turbulence are still not well established due in part to a lack of experimental correspondence. Here, we experimentally and numerically find that even a small, trapped, compressible superfluid can display characteristics analogous to those of classical 2D turbulence, suggesting a broader view of the universality of 2D turbulence. Regarding the possibility of a compressible superfluid supporting an inverse energy cascade, energy fluxes provide the most direct route to identifying cascades; while this remains an open problem for trapped BECs [12], there is numerical evidence for inverse cascades in 2DQT [16]. Our observations are also consistent with energy transport from small to large length scales near the end of the stir: (i) infrequent vortex dipole recombination indicates that there is little dissipation over a forcing range k_F to k_s; (ii) $E^i(k) \propto k^{-3}$ for $k > k_s$, a range that cannot support energy flux [14]; (iii) in conjunction with vortex clustering, kinetic energy spectral developments occur primarily for $k < k_s$; (iv) $E^i(k) \propto k^{-5/3}$ for $k < k_s$, a signature of an inertial range; and (v) energy accumulates in a large-scale mode that was unpopulated prior to small-scale forcing. These observations motivate further investigations of 2DQT, with future work focusing on energy fluxes, dissipation, inhomogeneities, and direct experimental observations of vortex dynamics.

We thank Colm Connaughton and Sergey Nazarenko for useful discussions. We acknowledge funding from the U.S. National Science Foundation Grants No. PHY-0855677, No. PHY-1205713, and No. DMS-0806762; the U.S. Army Research Office; the Marsden Fund; the Royal Society of New Zealand; the New Zealand Foundation for Research, Science, and Technology Contracts No. UOOX0801 and No. NERF-UOOX0703; and the Australian Research Council Discovery Project No. DP1094025.

*Present address: School of Mathematics and Physics, University of Queensland, Brisbane, Queensland 4072, Australia.

†To whom correspondence should be addressed. abradley@physics.otago.ac.nz

‡To whom correspondence should be addressed. bpa@optics.arizona.edu

[1] M. Lesieur, *Turbulence in Fluids* (Kluwer, Dordrecht, 1990), 4th ed.

[2] R. Kraichnan, Phys. Fluids **10**, 1417 (1967); C. Leith, Phys. Fluids **11**, 671 (1968); G. Batchelor, Phys. Fluids **12**, II-233 (1969); R. Kraichnan and D. Montgomery, Rep. Prog. Phys. **43**, 547 (1980).

[3] J. Sommeria, in *New Trends in Turbulence*, Proceedings of the Les Houches Summer School, Session LXXIV (EDP Sciences, Les Ulis, France, 2001), p. 385; P. Tabeling, Phys. Rep. **362**, 1 (2002); G. Boffetta and R. E. Ecke, Annu. Rev. Fluid Mech. **44**, 427 (2012).

[4] D. K. Lilly, J. Atmos. Sci. **40**, 749 (1983).

[5] M. G. Shats, H. Xia, and H. Punzmann, Phys. Rev. E **71**, 046409 (2005).

[6] J. Sommeria, S. D. Meyers, and H. L. Swinney, Nature (London) **331**, 689 (1988).

[7] J. Miller, P. B. Weichman, and M. C. Cross, Phys. Rev. A **45**, 2328 (1992).

[8] L. Onsager, Nuovo Cimento **6**, supplement to issue 2, 279 (1949).

[9] S. Nazarenko and M. Onorato, J. Low Temp. Phys. **146**, 31 (2007).

[10] T.-L. Horng, C.-H. Hsueh, S.-W. Su, Y.-M. Kao, and S.-C. Gou, Phys. Rev. A **80**, 023618 (2009).

[11] R. Numasato and M. Tsubota, J. Low Temp. Phys. **158**, 415 (2010).

[12] R. Numasato, M. Tsubota, and V. S. L'vov, Phys. Rev. A **81**, 063630 (2010).

[13] B. Nowak, J. Schole, D. Sexty, and T. Gasenzer, Phys. Rev. A **85**, 043627 (2012).

[14] A. S. Bradley and B. P. Anderson, Phys. Rev. X **2**, 041001 (2012).

[15] M. T. Reeves, B. P. Anderson, and A. S. Bradley, Phys. Rev. A **86**, 053621 (2012).

[16] M. T. Reeves, T. P. Billam, B. P. Anderson, and A. S. Bradley, Phys. Rev. Lett. **110**, 104501 (2013).

[17] K. Sasaki, N. Suzuki, and H. Saito, Phys. Rev. Lett. **104**, 150404 (2010).

[18] T. W. Neely, E. C. Samson, A. S. Bradley, M. J. Davis, and B. P. Anderson, Phys. Rev. Lett. **104**, 160401 (2010).

[19] S. J. Rooney, P. B. Blakie, B. P. Anderson, and A. S. Bradley, Phys. Rev. A **84**, 023637 (2011).

[20] Here, two-dimensionality refers to the fluid's velocity lying primarily in a plane throughout the system. Quasi-2D BECs ($\mu_0 < \hbar\omega_z$) are not necessary and are not used in our study.

[21] *Quantized Vortex Dynamics and Superfluid Turbulence*, edited by C. F. Barenghi, R. J. Donnelly, and W. F. Vinen (Springer, Berlin, 2001).

[22] W. F. Vinen and J. J. Niemela, J. Low Temp. Phys. **128**, 167 (2002).

[23] C. Raman, J. R. Abo-Shaeer, J. M. Vogels, K. Xu, and W. Ketterle, Phys. Rev. Lett. **87**, 210402 (2001).

[24] E. A. L. Henn, J. A. Seman, G. Roati, K. M. F. Magalhães, and V. S. Bagnato, Phys. Rev. Lett. **103**, 045301 (2009).

[25] Here, "pinning" refers to the spatial localization of vortex cores or fluid circulation due to local bumps in the trapping potential. In our experiments, the vortex core has an associated energy that is minimized when the vortex core overlaps with the zero-density region caused by the central potential.

[26] C. Ryu, M. F. Andersen, P. Cladé, V. Natarajan, K. Helmerson, and W. D. Phillips, Phys. Rev. Lett. **99**, 260401 (2007).

[27] C. N. Weiler, T. W. Neely, D. R. Scherer, A. S. Bradley, M. J. Davis, and B. P. Anderson, Nature (London) **455**, 948 (2008).

[28] See Supplemental Material at http://link.aps.org/supplemental/10.1103/PhysRevLett.111.235301 for additional information.

[29] A. Ramanathan, K. C. Wright, S. R. Muniz, M. Zelan, W. T. Hill, III, C. J. Lobb, K. Helmerson, W. D. Phillips,

and G. K. Campbell, Phys. Rev. Lett. **106**, 130401 (2011).
[30] S. Moulder, S. Beattie, R. P. Smith, N. Tammuz, and Z. Hadzibabic, Phys. Rev. A **86**, 013629 (2012).
[31] M. Kobayashi and M. Tsubota, Phys. Rev. Lett. **94**, 065302 (2005).
[32] P. B. Blakie, A. S. Bradley, M. J. Davis, R. J. Ballagh, and C. W. Gardiner, Adv. Phys. **57**, 363 (2008).
[33] L. P. Pitaevskii, Zh. Eksp. Teor. Fiz. **35**, 408 (1958).
[34] C. Nore, M. Abid, and M. E. Brachet, Phys. Fluids **9**, 2644 (1997).
[35] The spectrum $E^i(k)$ is a function of $k = |\mathbf{k}|$, obtained by integrating the 2D spectrum of incompressible energy over the azimuthal angle ϕ_k for $\mathbf{k} = k(\cos\phi_k, \sin\phi_k)$.
[36] A. N. Kolmogorov, Dokl. Akad. Nauk SSSR **30**, 301 (1941).
[37] A. C. White, C. F. Barenghi, and N. P. Proukakis, Phys. Rev. A **86**, 013635 (2012).
[38] T. P. Billam, M. T. Reeves, B. P. Anderson, and A. S. Bradley, arXiv:1307.6374.